Cell

Transport through the Golgi Apparatus by Rapid Partitioning within a Two-Phase Membrane System

George H. Patterson,[1,6] Koret Hirschberg,[3,6] Roman S. Polishchuk,[4] Daniel Gerlich,[5] Robert D. Phair,[2,6] and Jennifer Lippincott-Schwartz[1,*]

[1]Cell Biology and Metabolism Program, National Institutes of Health, Building 18T, Room 101, 18 Library Drive, Bethesda, MD 20892-5430
[2]Integrative Bioinformatics, Los Altos, CA, 94024
[3]Department of Pathology, Sackler School of Medicine, Tel-Aviv University, Tel-Aviv 69978, Israel
[4]Department of Cell Biology and Oncology, Consorzio "Mario Negri Sud" Santa Maria Imbaro, Chieti 66030, Italy
[5]ETH Zurich, Institute of Biochemistry, HPM D11.3, Schafmattstrasse 18, 8093 Zurich, Switzerland
[6]These authors contributed equally to this work
*Correspondence: lippincj@mail.nih.gov
DOI 10.1016/j.cell.2008.04.044

SUMMARY

The prevailing view of intra-Golgi transport is cisternal progression, which has a key prediction—that newly arrived cargo exhibits a lag or transit time before exiting the Golgi. Instead, we find that cargo molecules exit at an exponential rate proportional to their total Golgi abundance with no lag. Incoming cargo molecules rapidly mix with those already in the system and exit from partitioned domains with no cargo privileged for export based on its time of entry into the system. Given these results, we constructed a new model of intra-Golgi transport that involves rapid partitioning of enzymes and transmembrane cargo between two lipid phases combined with relatively rapid exchange among cisternae. Simulation and experimental testing of this rapid partitioning model reproduced all the key characteristics of the Golgi apparatus, including polarized lipid and protein gradients, exponential cargo export kinetics, and cargo waves.

INTRODUCTION

The Golgi apparatus processes and sorts newly synthesized protein and lipid moving through the secretory pathway (Kepes et al., 2005). It is typically composed of seven flattened cisternae arranged as an asymmetric stack with surrounding vesicles and tubules (Ladinsky et al., 1999). The *cis* or forming face has cisternae morphologically and biochemically similar to the endoplasmic reticulum (ER). The *trans* or distal face at the opposite pole contains cisternal membranes that resemble the plasma membrane and associate with forming secretory vesicles. Within the stack, lipids and proteins maintain *cis*-to-*trans* gradients in distributions (Holthuis et al., 2001; Orci et al., 1981; Rabouille et al., 1995; Roth et al., 1986) despite continuous movement of secretory cargo through the system.

The most widely accepted model for how the Golgi apparatus accomplishes its diverse and essential trafficking tasks is cisternal progression (or maturation). It postulates that the stack of Golgi cisternae constitute a historical record of progression from entry at the *cis* face to exit at the *trans* face (Glick et al., 1997). Recently arrived cargo molecules are confined to the *cis*-most cisterna, undergo initial processing, and await arrival of enzymes from more distal cisternae for subsequent processing. In this model, cargo molecules remain within a given cisterna as it passes, conveyor-belt-like, through an average of seven locations within the Golgi stack on its way to the *trans* face and exit from the Golgi via transport carriers. Data from electron microscopy studies of large cargo proteins like Procollagen (Bonfanti et al., 1998) or scale formation in algae (Melkonian et al., 1991) have been interpreted to show these molecules traversing the stack without leaving their cisternal cocoon. Observations of cargo transport after a temperature block indicate a wave-like distribution that has been interpreted as cisternae with confined cargo progressing across the stack (Trucco et al., 2004). In addition, the sequential appearance of Golgi enzymes in individual yeast cisterna over time (Losev et al., 2006; Matsuura-Tokita et al., 2006) has been widely cited in support of this hypothesis.

Here, we report the results from fluorescent highlighting experiments that pose a challenge to cisternal progression in its classic form. The data revealed that newly arrived cargo in the Golgi exited with exponential kinetics rather than exhibiting a discrete lag or transit time as predicted by cisternal progression. Moreover, transmembrane cargo molecules entering the Golgi quickly distributed throughout the system before differentially partitioning between two different membrane environments: processing domains enriched in Golgi enzymes and export domains capable of budding transport intermediates. To develop a model consistent with these data, we propose that intra-Golgi trafficking is based on partitioning of transmembrane cargo and enzymes within a two-phase membrane system. Through experimental testing and simulation, this model is found to explain the full range of Golgi characteristics, including polarized lipid and protein gradients, exponential cargo export kinetics, and cargo waves.

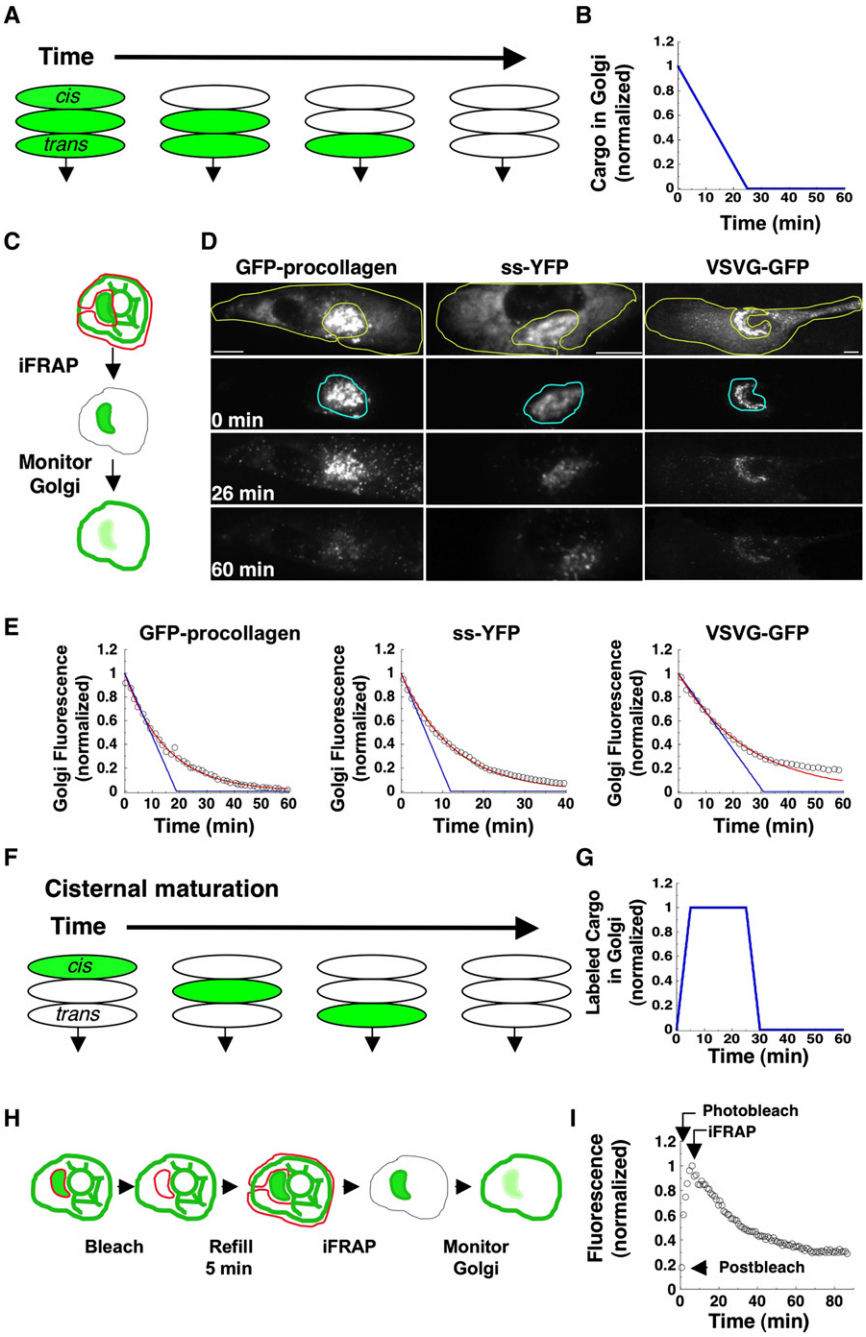

Figure 1. Cargo Exit Kinetics from the Golgi Show an Exponential Rather Than Linear Loss of Cargo

(A) Diagram of cisternal progression in its classical form modeled as newly arrived cargo, moves forward, and exits.

(B) Simulation of cargo export for a pool of cargo initially distributed throughout the Golgi apparatus and assuming a 25 min transit time. Details of model implementation are in Model S1.

(C) Inverse FRAP (iFRAP) was employed to selectively highlight Golgi cargo molecules.

(D) The indicated cargo molecules expressed in human fibroblasts, NRK, and COS7 cell types were subjected to iFRAP (yellow regions) and monitored over time. Scale bars represent 10 μm.

(E) Golgi region fluorescence (outlined in blue in [D]) was then monitored at 1 min intervals and plotted over time. The open circles represent Golgi fluorescence associated with each cargo type after the iFRAP. The mean Golgi fluorescence values were normalized to the first data point after the iFRAP. The best fit of the data predicted for the cisternal-progression model is shown in blue. The observed kinetics of export were best described by an exponential decrease (in red) with fits yielding distinct exit rate constants of 0.065 min^{-1} for GFP-Procollagen, 0.039 min^{-1} for VSVG-GFP, and 0.07 min^{-1} for ss-YFP. Details of model implementation and data fitting are in the Model S1.

(F) Diagram of a 5 min input of cargo in the cisternal-progression model.

(G) Simulation of the 5 min pulse protocol showing the Golgi fluorescence as predicted by 25 min cisternal progression. Details of model implementation are in Model S2.

(H) Photobleaching protocol to monitor a 5 min pulse of VSVG-YFP fluorescence within the Golgi. Cells were shifted from 40°C to 32°C for 25 min to accumulate a pool VSVG-YFP in the Golgi. This pool was photobleached, and molecules from the ER entered the Golgi for 5 min before an iFRAP was performed.

(I) COS 7 cells expressing VSVG-YFP were subjected to the experiment outlined in (H). Open circles represent the mean Golgi fluorescence at each time point. The data are normalized to the time point immediately after the iFRAP.

RESULTS

iFRAP to Measure Bulk Golgi Exit Kinetics

A salient prediction made by the classical cisternal-progression model is that a pool of cargo initially distributed throughout the stack empties with time in a linear fashion in the absence of further input (Figures 1A and 1B, details in Model S1 and Figure S1, available online). Linear export kinetics are predicted because the cisternae conveying cargo are thought to form at the *cis* face, move across the stack, and be consumed into vesicles at the *trans* face at a constant rate. So that this prediction could be tested, the export kinetics of three different types of GFP-tagged cargo molecules (large soluble, small soluble, and transmembrane) were examined. GFP-Procollagen, which assembles into aggregates upon arrival in the Golgi from the ER (Bonfanti et al., 1998), was used as large, soluble cargo, whereas YFP with a cleavable signal sequence peptide (ss-YFP) (Nehls et al., 2000) was used as small, inert soluble cargo. The temperature-sensitive ts045 VSVG protein (VSVG-GFP), which is retained in the ER at 40°C and moves into the secretory pathway

at 32°C, was used as transmembrane cargo (Presley et al., 1997). After expressing these proteins in cells and establishing their steady-state distribution through the secretory pathway at 32°C, we selectively highlighted the cargo pool in the Golgi by photobleaching all fluorescent molecules outside the Golgi region with a technique referred to as inverse fluorescence recovery after photobleaching (iFRAP) and then monitored by time-lapse imaging. (Figure 1C)

Representative images from iFRAP experiments on cells expressing each type of cargo protein are shown in Figure 1D (see Movies S1–S3). When the fluorescent intensities associated with the Golgi region of interest (outlined in blue) are plotted over time (Figure 1E, open circles), no cargo type exhibits the linear export kinetics predicted by the classical cisternal-progression model (Figure 1E, blue lines; for details see Model S1 and Figure S1A). Instead, all cargo types show exponential efflux kinetics and can be fit with a single Golgi exit rate constant (Figure 1E, red curves). (Because each cargo is expressed in a different cell type, the relative difference among the rate constants is not informative.)

For GFP-Procollagen and ss-YFP, the fits to a single first order process have average coefficients of variation for the effective rate constants well below 5%. For VSVG-GFP, the fit diverges slightly at late time points possibly because of slow endocytosis and delivery of VSVG-GFP to juxtanuclear endosomes within the Golgi region after arrival at the plasma membrane. Repeated iFRAP over the time course results in no divergence from a single exponential process of Golgi cargo efflux, confirming this explanation (data not shown). Tests of other GFP-tagged transmembrane cargo proteins, including Tac-GFP and NTCP-GFP (Na^{2+} taurocholate cotransporting polypeptide) (Sun et al., 2001), also exhibit exponential Golgi efflux kinetics (see Figure S9). The average residence time of the different cargos in the Golgi (calculated as the inverse of their rate constants) range from 15 min for ss-YFP to 25 min for VSVG-GFP, which are well within the range estimated from biochemical experiments (Fries et al., 1984). The results are thus inconsistent with a linear export process and instead point to an export mechanism compatible with exponential release.

Cargo Export Kinetics after a 5 Min Pulse Labeling

Besides linear export, the classical cisternal-progression model predicts a lag before newly arrived cargo is exported from the Golgi (Figure 1F). This prediction follows from the view of the cisternal progression model that cargo-laden cisternae pass vectorially through multiple locations within the Golgi stack on their way to the *trans* face, where cargo can exit from the Golgi. In the case of a 25 min cisternal-progression time, therefore, if labeled cargo is pulsed into the Golgi over a 5 min period, no label should be seen exiting the Golgi for at least another 20 min (Figure 1G; details in Model S2 and Figure S1B).

To test this prediction, we employed a protocol to fluorescently label an incoming pool of VSVG molecules that had only been in the Golgi for 5 min (Figure 1H). The results from this experiment reveal that the pulse-labeled pool of VSVG-GFP exited the Golgi with exponential kinetics, exhibiting no lag before fluorescent VSVG-GFP molecules left the Golgi (Figure 1I). Newly arrived VSVG-GFP molecules and VSVG-GFP molecules already present in the Golgi have similar probabilities of exit. As with our findings on bulk cargo release, therefore, the results on pulsed cargo release point to a mechanism yielding exponential rather than linear cargo release from the Golgi.

The Cisternal-Progression Model with Variable Cargo Transit Times Still Cannot Explain the Kinetic Results

To reconcile the observed exponential patterns of Golgi cargo release with the cisternal-progression model, we examined several possible variations. The first was based on the observation that many cells have numerous Golgi stacks, which could have different cargo transit times because of differences in cisternal-progression times. When averaged together, this could give rise to the observed exponential efflux kinetics.

This variation is illustrated for 100 stacks having a symmetric distribution of transit times ranging from 19 to 31 min centered around the observed 25 min mean residence time for VSVG-GFP (Figure 2A; details in Model S3 and Figure S2A). The simulation yields a roughly linear profile (blue curve), similar to the simple conveyor belt model of a fixed transit time of 25 min (green curve) but punctuated by sudden small declines as each group of stacks release its cargo to export. The lag of 2.9 min preceding the initial cargo loss reflects the time required for the *trans*-most cisterna to empty in the fastest group of stacks. Thus, this scenario cannot reproduce exponential export kinetics (shown by the dashed curve, Figure 2A).

EM Shows Rapid Filling of Golgi Stacks and No Cargo Enrichment in the *trans*-Most Cisterna

Given that a distribution of Golgi transit times cannot explain the export kinetics data, we considered a second variation of the classical model. In this variation, cargo-containing cisternae progress quickly across the stack and fuse with the *trans*-most cisterna, and cargo is then exported by a single rate-limiting process. Exponential export kinetics is possible in this scenario if cisternae progress across the stack quickly enough so that newly arrived and pre-existing cargo become well mixed in the *trans*-most cisterna on a time scale faster than export. This necessarily predicts concentration of cargo in the *trans*-most cisterna (details in Model S4 and Figure S2B). We tested this using immunogold labeling and electron microscopy in cells expressing VSVG-GFP that were shifted from 40°C to 32°C (Figure 2B).

Prior to the temperature shift, virtually no gold particles are found in the Golgi area, consistent with retention of VSVG in the ER at the restrictive temperature. Within 5 min of shift to the permissive temperature (32°C), gold labeling for VSVG-GFP is found throughout the Golgi stack (for quantification, see Figure S2C). This indicates that VSVG-GFP moves efficiently from ER to Golgi at 32°C and upon arriving in the Golgi can rapidly move throughout the organelle. Notably, VSVG-GFP maintains a widespread distribution in the Golgi without concentrating in the *trans*-most or any other cisterna, even at later time points when input from the ER decreased (Figure 2B, 50 min; Figure S2C). The data are thus inconsistent with a variation of cisternal progression in which cargo-laden cisternae progress quickly across the stack, delivering their cargo to the *trans*-most cisterna, where it is retained for later export by a rate-limiting process.

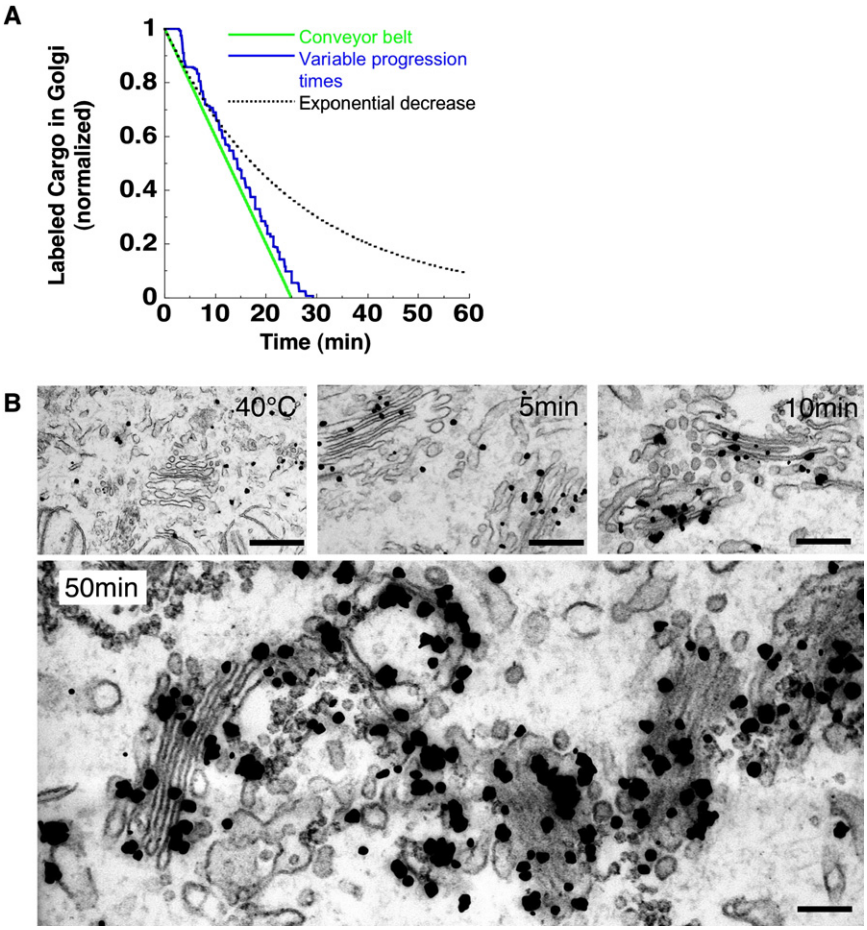

Figure 2. Simulation of the Cisternal-Progression Model Modified to Include Variable Transit Times and Electron Microscopy of VSVG Filling the Golgi Apparatus

(A) Cisternal progression modeled as a conveyor belt (green line) with a transport delay of 25 min with an iFRAP protocol. Cisternal progression is modeled as a population of 100 Golgi stacks having a symmetrical distribution of transport times centered around 25 min with an iFRAP protocol (blue line). Cargo export is modeled as an exponential decrease with an iFRAP protocol (dashed line). See Model S3 for details.

(B) VSVG-GFP was expressed in COS 7 cells at 40°C (scale bar, 480 nm) and shifted to 32°C for 5 (scale bar, 300 nm), 10 (scale bar, 300 nm), and 50 (scale bar, 120 nm) min before fixation and processing for immunogold-electron microscopy.

The Cisternal-Progression Model Modified to Include Extensive Cargo Recycling

A third variation of the cisternal-progression model includes cargo recycling. So that this alternative hypothesis could be tested, iFRAP responses were simulated as the recycling fraction of cargo (from the *trans* face of each cisterna to the *cis* face of all preceding cisternae) varied between 1% and 30% (Figures 3A and 3B; details in Model S5 and Figure S3). The plots for 1%–20% do not fit the observed exponential kinetics, having prominent shoulders in the semilog plots (Figure 3B) reflecting the time for cargo-laden cisternae to traverse the stack. But for 30% and larger recycling fractions, cisternal progression begins to approach exponential export kinetics as observed with the iFRAP data.

The 30% recycling rate, however, requires rapid cisternae transit across the Golgi stack to achieve the observed 25 min residence time for VSVG-GFP and results in cargo quickly approaching a well-mixed state across the stack. This is illustrated in Figure 3C, which shows simulated cisternal progression with 30% recycling for a pulse of cargo added to the first cisterna of a seven-cisterna stack. The effect of this fast progression and recycling is that a pulse of cargo introduced at the *cis*-most cisterna becomes well distributed across the stack within ~6 min, making the Golgi an effectively well-mixed compartment.

This leads to inconsistencies with previous data supporting cisternal progression. Notably, the high rate of recycling makes it impossible for cisternal progression to reproduce a wave of cargo moving across the stack over ~12–16 min (Trucco et al., 2004). The fast recycling causes the model to lose its maturation character because of the mixing of cargo contents within 6 min of their entry (Figure 3C). Reduction of the recycling rate can yield a cargo wave, as shown for cisternal progression modeled with 1% recycling (Figure 3D), but overall export kinetics are not exponential (Figures 3A and 3B) because of the slow rate of cisternal progression. Hence, cisternal progression with either low or high recycling rates cannot simultaneously account for the exponential export kinetics data reported here and the cargo wave data seen in temperature shift experiments (Trucco et al., 2004).

Two-Color Imaging Suggests a Membrane Partitioning Model

In attempts to overcome these difficulties, we utilized dual time-lapse imaging and photobleaching to observe the spatial organization and dynamics of membrane cargo and resident enzymes within the Golgi more precisely. Previous live-cell imaging work has shown that transmembrane cargo and enzymes in the Golgi laterally segregate into discrete domains (White et al., 2001). These domains are unlikely to correspond to distinct cisternae within a Golgi stack (i.e., *cis* versus *trans*) because the distance across a stack (~130 nm) is well below the resolution limit of diffraction-limited confocal microscopy. To verify that transmembrane cargo and Golgi enzymes spatially segregate into optically distinguishable domains in our system, we selectively photobleached the VSVG-YFP molecules in the Golgi within cells expressing VSVG-YFP and GalT-CFP and then compared the distribution of newly arrived, fluorescent VSVG-YFP molecules from the ER to that of the Golgi marker (Figure 4A and Movie S4).

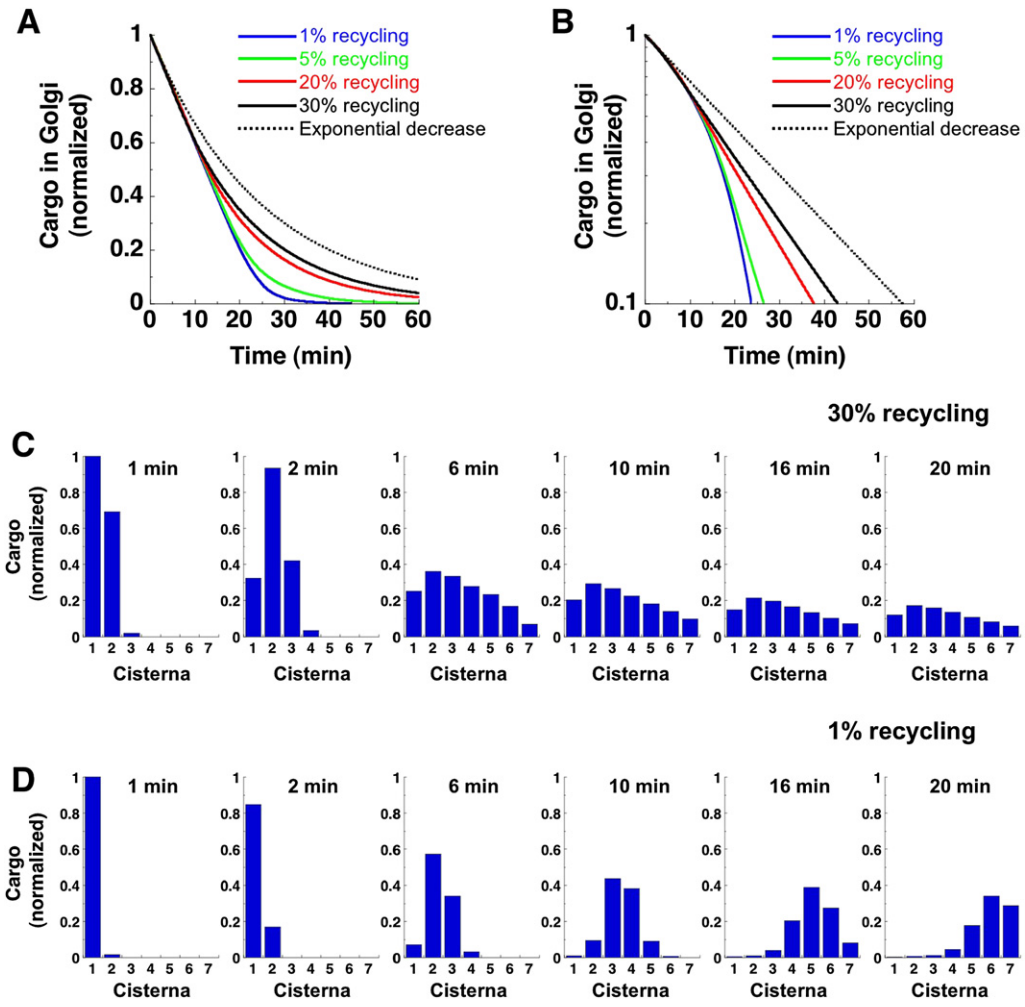

Figure 3. Predicted Export Kinetics for the Cisternal-Progression Model Modified to Include Cargo Recycling

(A) Golgi iFRAP experiments were simulated as the recycling fraction of cargo (from the *trans*-most cisterna to all preceding cisternae) was varied between 1% and 30%. An exponential decrease is modeled as a single compartment with first-order exit.

(B) The simulations in (A) are displayed on a semilog plot to illustrate the monotonically increasing slope of the cisternal progression simulations.

(C) A pulse of cargo molecules introduced into the *cis*-most cisterna of a seven-cisterna stack is simulated as the cargo moves through the Golgi with 30% recycling and a 25 min residence time. The fraction of cargo molecules found in each cisterna relative to the initial cisterna 1 amount is shown at the indicated time points after the pulse.

(D) A pulse of cargo molecules introduced into the *cis*-most cisterna is simulated as it passes through the Golgi by cisternal progression with 1% recycling. As in (C), the fraction of cargo molecules found in each cisterna is displayed. See Model S5 for details.

VSVG-YFP (green) rapidly redistributes into areas containing GalT-CFP (red) upon arriving at the Golgi. Domains of VSVG-YFP enrichment relative to GalT-CFP can be observed at all subsequent times during VSVG-YFP transport through the Golgi (Figure 4A, images; Movie S5). This is confirmed by measurement of the relative intensities of VSVG-YFP and GalT-CFP within a line drawn across the Golgi (Figures 4A and 4B, graphs). Segregated domains are not observed in cells expressing two colors of the same proteins (Figures 4C and 4D). Transport intermediates containing VSVG-YFP molecules bud from the domains of VSVG-YFP enrichment (Movie S5). Similar results are obtained when VSVG-YFP is coexpressed with two other Golgi markers, sialyltransferase (ST) and mannosidase II (Man II) (Figure S10). These observations raise the possibility that upon entering the Golgi, VSVG molecules are rapidly partitioned between two domains, one enriched in processing enzymes and one that is not, and that these two domains are maintained over extended periods (>20 min) as cargo is exported from the system.

Partitioning Model Suggests an Experimental Test for Exchange

The minimal model diagrammed in Figure 5A was constructed without the features of cisternal progression to test the consistency of partitioning with the observed exponential efflux kinetics. In this scheme, transmembrane cargo molecules like VSVG move between two different Golgi membrane locations, a processing domain enriched in Golgi enzymes, and an export

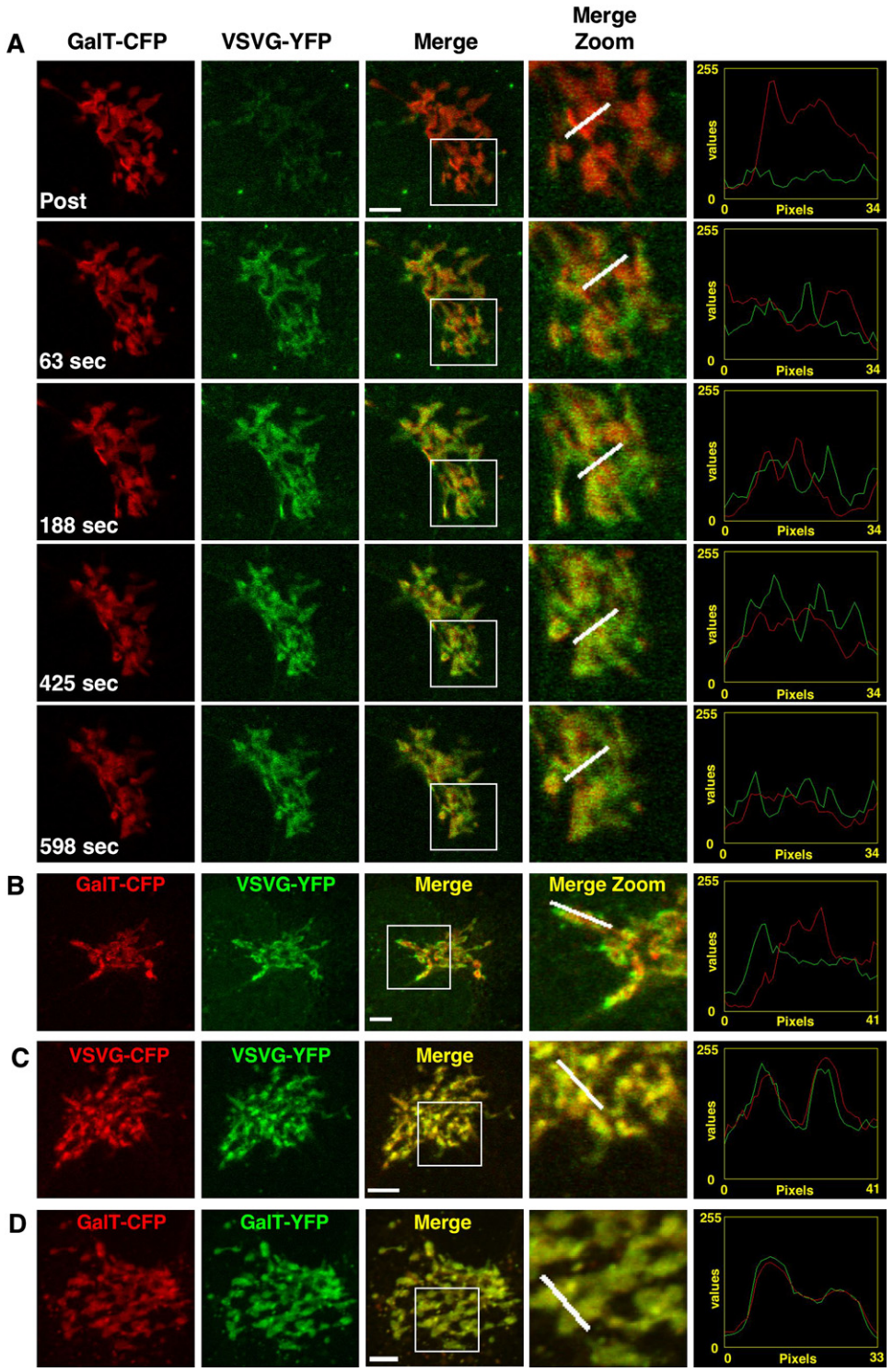

Figure 4. Two-Color Imaging Reveals Cargo and Enzyme Domains of the Golgi

(A) COS 7 cells expressing GalT-CFP and VSVG-YFP were shifted from 40°C to 32°C for 15 min to accumulate VSVG-YFP within the Golgi. The Golgi population of VSVG-YFP was photobleached (post), and ER-derived, nonphotobleached VSVG-YFP molecules entering the Golgi were monitored at ~16 s intervals. The GalT-CFP (red) and VSVG-YFP (green) images are shown in columns 1 and 2, respectively with merged images in column 3. The scale bar in the merged image represents 5 μm. A magnified view of the merged image is shown in column 4. Images were contrast enhanced linearly to the full dynamic range of the brightest postbleach image in either the GalT-CFP or VSVG-YFP time series and applied to the entire data set. Line profiles of the CFP (red) and YFP (green) fluorescence intensities from the lines in the magnified views are shown in column 5.

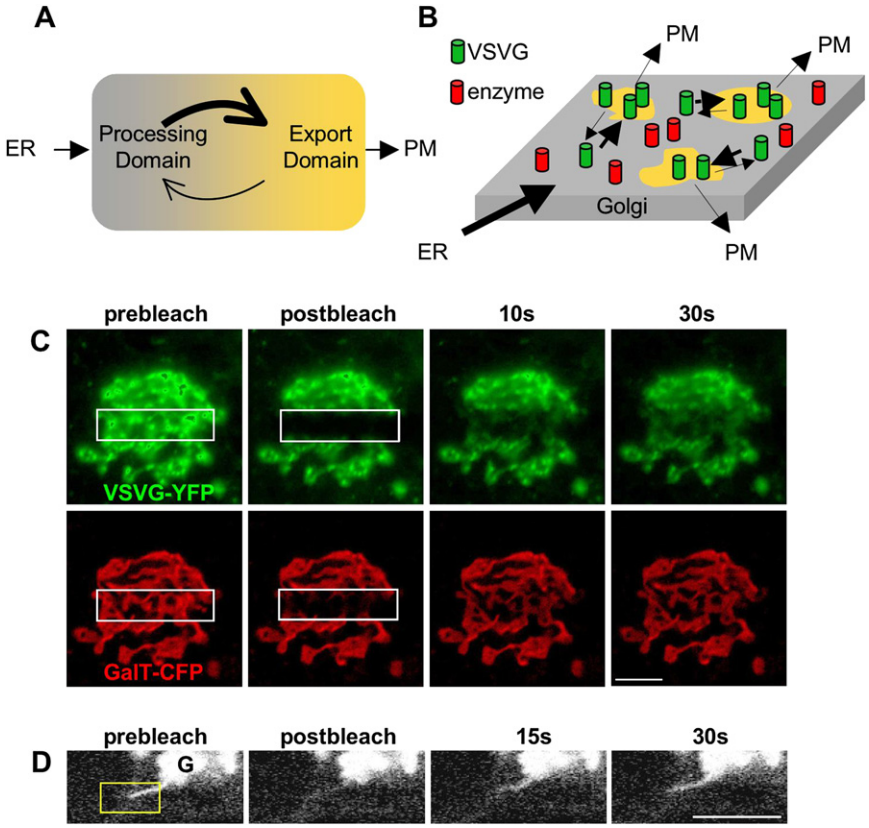

Figure 5. VSVG Diffuses into and out of Golgi Export Domains

(A) Model depicting partitioning of VSVG-YFP between two phases of the Golgi (processing domain and export domain).

(B) Cartoon depicting partitioning model for a small region of Golgi membrane. The green cylinders represent VSVG and red cylinders represent resident Golgi enzymes. The regions indicated in yellow represent Golgi export domains.

(C) Human fibroblasts expressing VSVG-YFP and GalT-CFP were shifted from 40°C to 32°C for 35 min to accumulate VSVG-YFP within the Golgi. The Golgi populations of GalT-CFP (red) and VSVG-YFP (green) were subjected to photobleaching within the regions indicated in the rectangles and imaged at 1 s intervals.

(D) COS 7 cells expressing VSVG-GFP were shifted from 40°C to 32°C for 40 min to accumulate a pool within the Golgi. The forming tubule was photobleached and its recovery imaged at 15 s intervals. Scale bars represent 5 μm.

domain from which transport intermediates bud from the Golgi. Explaining the exponential efflux kinetics reported in Figure 1, requires only that exchange of VSVG between these two membrane domains be faster than export. Every VSVG molecule then has essentially the same probability of being incorporated into transport intermediates even though they are constantly exchanging between domains (see Figure 5B). If the partitioning or equilibration constant between processing and export domains for VSVG also favored export domains, then VSVG's exponential efflux kinetics and export domain enrichment would be explained by the same simple mechanism.

To test this partitioning scheme, we photobleached a box across the Golgi region in cells coexpressing VSVG-YFP and GalT-CFP. Fluorescence from both molecules quickly replenishes the bleached area, but VSVG-YFP replenishment occurs more slowly (Figure 5C), as predicted if VSVG-YFP molecules partition into and out of membrane export domains while also circulating within processing domains. Supporting this, when a tubule containing VSVG-YFP that mediates export from the Golgi is photobleached (Figure 5D), the level of replenished fluorescence reaches comparable levels to the pre-existing fluorescence in the tubule. The incomplete photobleaching provides confirmation that the tubule does not detach from the Golgi and re-emerge but is simply refilling with VSVG-YFP fluorescence. Undetached tubules neither become brighter with time nor exceed the average Golgi fluorescence, so exchange with the Golgi is clearly bidirectional. These data thus suggest that VSVG undergoes continuous, selective partitioning between processing and export domains upon entering the Golgi.

Enzymes and Transmembrane Cargo in the Golgi Differentially Segregate in Response to Brefeldin A

Further evidence for a partitioning model comes from examination of the behaviors of GalT-CFP and VSVG-YFP during brefeldin A treatment, which causes Golgi enzymes to return to the ER and causes the Golgi to disassemble (Lippincott-Schwartz et al., 1991). A portion of VSVG-YFP does not redistribute to the ER with GalT-CFP during Golgi disassembly but remains in the Golgi region and continues to be packaged into transport carriers directed toward the plasma membrane (Figure 6A; Movie S6). Three observations indicate that this results from a partitioning mechanism rather than localization of VSVG-YFP within a brefeldin A (BFA)-resistant trans-Golgi network (TGN) (Lippincott-Schwartz et al., 1991). First, the soluble cargo protein, ss-YFP,

(B) COS 7 cells expressing GalT-CFP (red) and VSVG-YFP (green) were shifted from 40°C to 32°C for 30 min to accumulate VSVG-YFP within the Golgi. A magnified view of the merged image is shown in column 4.

(C) COS 7 cells expressing VSVG-CFP (red) and VSVG-YFP (green) were shifted from 40°C to 32°C for 30 min to accumulate a Golgi pool. A magnified view of the merged image is shown in column 4.

(D) COS 7 cells expressing GalT-CFP (red) and GalT-YFP (green) were shifted from 40°C to 32°C for 30 min before imaging. A magnified view of the region indicated by the square in the merged image is shown in column 4. Images were contrast enhanced linearly to the full dynamic range. Line profiles of the CFP (red) and YFP (green) fluorescence intensities from the line in the magnified view in (B), (C), and (D) are shown in column 5. Scale bars in the merged images of (B), (C), and (D) represent 5 μm. The CFP and YFP variants were Cerulean (Rizzo et al., 2004) and Venus (Nagai et al., 2002), respectively.

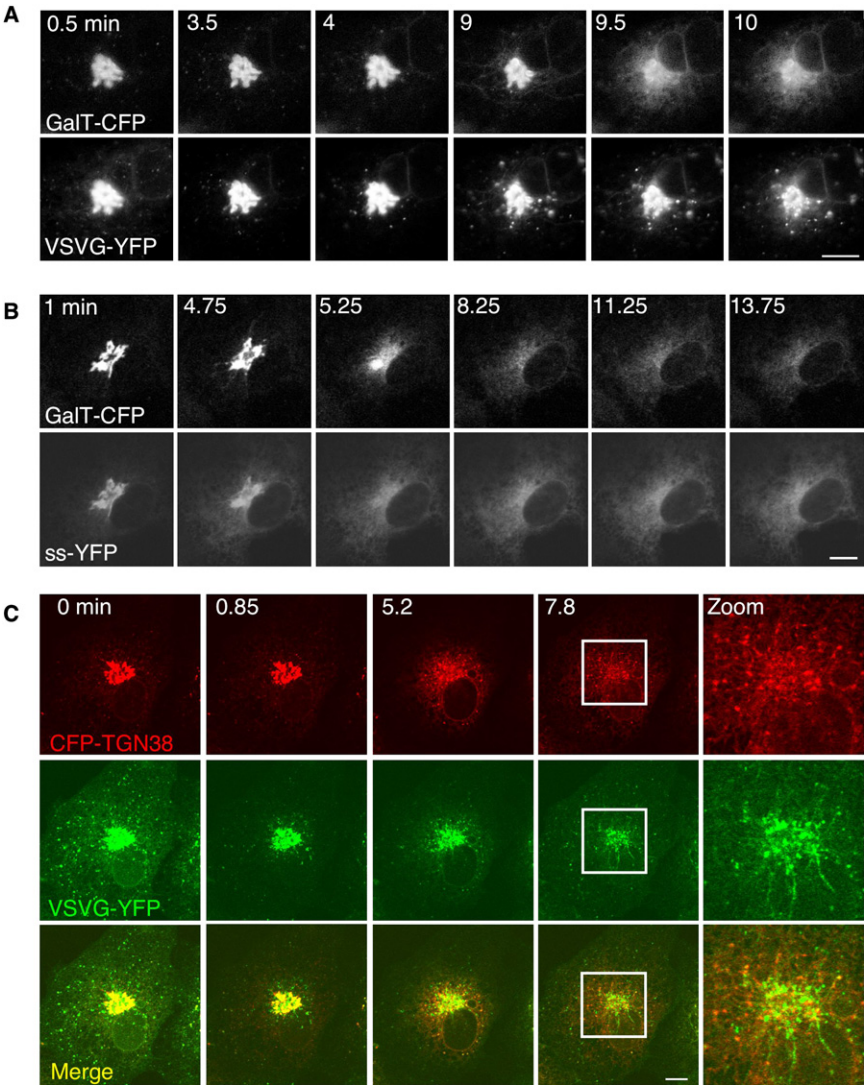

Figure 6. Disruption of the Golgi with Brefeldin A during Cargo Transport Demonstrates Enzyme and Export Domains of the Golgi

(A) COS 7 cells expressing VSVG-YFP and GalT-CFP were shifted from 40°C to 32°C for 30 min to accumulate a Golgi pool of VSVG-YFP. Brefeldin A (5 μg/ml) was added, and and the Golgi region was highlighted by iFRAP. Images of VSVG-YFP and GalT-CFP were acquired at 30 s intervals as the Golgi redistributed into the ER.

(B) COS 7 cells expressing ss-YFP and GalT-CFP were shifted from 40°C to 20°C for 2 hr to accumulate ss-YFP within the Golgi. BFA (5 μg/ml) was added, and the Golgi region was highlighted by iFRAP. The ss-YFP and GalT-CFP were imaged at ~16 s intervals as the Golgi redistributed into the endoplasmic reticulum.

(C) COS 7 cells expressing CFP-TGN38 (red) and VSVG-YFP (green) were shifted from 40°C and to 32°C for 30 min to accumulate a Golgi pool of VSVG-YFP. Brefeldin A (5 μg/ml) was added and the Golgi region was highlighted by iFRAP. Images of VSVG-YFP and CFP-TGN38 were acquired at ~16 s intervals as the Golgi redistributed into the ER. The CFP and YFP variants used in (C) were Cerulean (Rizzo et al., 2004) and Venus (Nagai et al., 2002), respectively. Scale bars represent 10 μm.

with no mechanism for selective membrane partitioning into BFA-resistant Golgi domains, rapidly redistributes back into the ER during BFA treatment with no portion remaining in the Golgi region (Figure 6B). Second, the amount of VSVG-YFP within Golgi export domains that resist return to the ER during BFA treatment does not noticeably change when BFA is added at 10 min or at 50 min after temperature shift from 40°C to 32°C (data not shown), conditions in which VSVG-YFP molecules will spend different lengths of time in the Golgi. And third, VSVG-YFP that resists return to the ER during BFA treatment does not colocalize with the TGN marker, TGN38 (Figure 6C). During intra-Golgi transport, therefore, transmembrane cargos like VSVG appear at all times to be partitioning between two distinct membrane environments: one characteristic of Golgi enzymes (i.e., processing domain), which is BFA sensitive; and one characteristic of Golgi export (i.e., export domain), which is BFA resistant and distinct from TGN38-containing membranes.

Developing the Membrane Partitioning Model of Golgi Organization and Trafficking

To give more definition to the Golgi partitioning model, we developed a spatially resolved version of it drawing on a number of observed features of the Golgi and model membrane systems (Figure 7A; Model S6; Figure S4). First, the lipid components in the two Golgi phases (i.e., processing and export) are considered either characteristic of ER and enriched in glycerophospholipids (GPL) (Model S7) or characteristic of plasma membrane and enriched in sphingolipids (SL) (Model S8) (Holthuis et al., 2001; van Meer and Sprong, 2004) with each type entering and exiting the Golgi by different routes (Gkantiragas et al., 2001; Holthuis et al., 2001; van Meer and Sprong, 2004). Vesicle-tubule mediation of protein and lipid traffic (Marsh et al., 2004; Orci et al., 2000; Trucco et al., 2004) is built into the model using intercisternal transport rates that prevent formation of a completely well-mixed system. We additionally hypothesized that budding of cargo toward the plasma membrane is not restricted to the *trans*-most cisterna, consistent with previous electron microscopy studies showing cargo-laden vesicles budding from all cisternae (Mogelsvang et al., 2004; Volchuk et al., 2000). Finally, transmembrane cargo proteins (see Model S9) and resident enzyme proteins (see Model S10) are modeled with preferential affinity for different SL/GPL compositions (Bretscher and Munro, 1993; Lundbaek et al., 2003), which is observed for proteins in artificial membrane systems (Killian, 1998). Thus, the Golgi partitioning model consists of cisternae

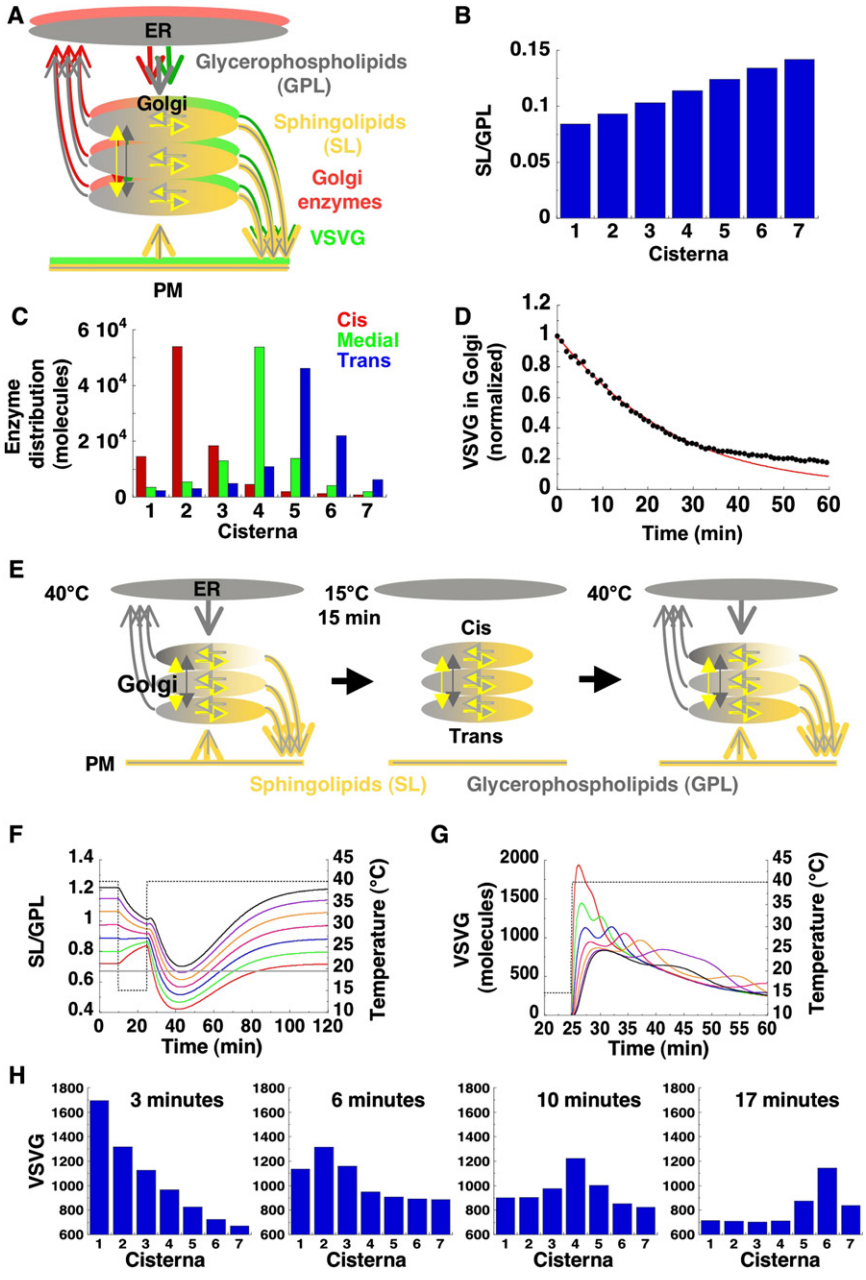

Figure 7. Development of the Rapid-Partitioning Model of Golgi Apparatus Organization and VSVG Transport

(A) The rapid-partitioning model consists of seven stages, of which only three are shown here for simplicity. Each stage represents one cisterna of an EM-resolved or biochemically resolved Golgi stack. The Golgi membrane lipid environment is modeled as having one component consisting of glycerophospholipids (GPL; gray) and another component consisting of cholesterol and glycosphingolipids (SL; yellow) giving rise to processing domains (gray) and export domains (yellow), respectively. Transmembrane cargo proteins move between both lipid environments but concentrate in the export domain (green), whereas transmembrane Golgi enzymes are excluded from export domains and diffuse within the processing domain (red).

(B) The steady-state ratio of sphingolipid (SL) and glycerophospholipid (GPL) levels is shown for each Golgi cisterna in a stack of seven cisternae upon simulation of the rapid-partitioning model constrained by literature data on organellar lipid abundances.

(C) Resident Golgi proteins distribute by partitioning into lipid domains of optimal composition. Simulations of trans Golgi proteins (dark blue), which are assumed to prefer higher SL/GPL environments than medial Golgi proteins (green) and *cis* Golgi proteins (red), result in polarized distributions of Golgi proteins across different cisternae.

(D) Rapid-partitioning model simulation (red line) of VSVG-GFP export during an iFRAP experiment is compared with the experimental data (black circles). Fit obtained by least squares. See Models S6–S10 for details.

(E) The small pulse 40°C-15°C-40°C experimental protocol used in a previous report (Trucco et al., 2004) was simulated for the rapid-partitioning model. The GPL (gray) and SL (yellow) distributions are illustrated for each temperature.

(F) SL/GPL ratios (left axis) in the Golgi exit domains are shown for cisterna 1 (red line), cisterna 2 (green line), cisterna 3 (blue line), cisterna 4 (magenta line), cisterna 5 (orange line), cisterna 6 (purple line), and cisterna 7 (black line). The temperature is indicated by the dashed black line (right axis), and the horizontal gray line indicates the SL/GPL ratio hypothesized to be optimal for VSVG partitioning.

(G) The number of VSVG molecules (left axis) is indicated for cisterna 1 (red line), cisterna 2 (green line), cisterna 3 (blue line), cisterna 4 (magenta line), cisterna 5 (orange line), cisterna 6 (purple line), and cisterna 7 (black line) during the 40°C-15°C-40°C protocol. The temperature is indicated by the dashed black line (right axis).

(H) The number of VSVG molecules located in each cisterna is shown for 3, 6, 10, 17 min after the shift from 15°C to 40°C. See Model S12 for more details.

with discrete processing and exit domains characterized by specialized lipid environments that differentially retain resident and cargo proteins based on thermodynamic partitioning.

Simulation of the Rapid-Partitioning Model Produces a Lipid Gradient, Nonuniform Enzyme Distributions, and Exponential Cargo Release

To test this rapid-partitioning model, we asked whether it could account in a quantitative manner for key characteristics of Golgi transport and organization, such as *cis*-to-*trans* gradient of glycerophospholipids (GPLs) and sphingolipids (SLs) (Holthuis et al., 2001; van Meer and Sprong, 2004), concentration of Golgi resident proteins in *cis*, medial, or *trans* regions (Dunphy and Rothman, 1983; Roth et al., 1986; Slot and Geuze, 1983), and exponential cargo release. This requires the spatially resolved form of the model because each of the key characteristics being tested refers to the spatial distribution of proteins and lipids within the Golgi apparatus.

After constraining the model with literature data on cellular GPL and SL compositions for ER, Golgi, and plasma membrane (details in Models S7 and S8), we found that it yields a steady-state *cis*-to-*trans* gradient in SL/GPL ratio across the Golgi stack (Figure 7B; details in Model S11 and Figure S5), which is dependent on a variety of features. For example, the gradient collapses when the lipids are forced to enter the Golgi randomly or when entry of the lipids into the Golgi is blocked. Likewise, the gradient does not form if transport across the stack is fast enough to cause the Golgi to be completely well mixed. Faster export from Golgi export domains to the plasma membrane increases the SL gradient and decreases the GPL gradient. In addition, faster recycling of GPL from Golgi processing domains to the ER increases the magnitude of the GPL gradient. The rapid-partitioning model thus generates *cis*-to-*trans* Golgi lipid gradients purely on the basis of the physical consequences of lipid partitioning, the organization of cellular lipid traffic, and the existence of intercisternal membrane traffic.

To explain the distribution of resident Golgi proteins within the stack, we hypothesized that these proteins distribute by partitioning into lipid domains of optimal composition. In brief, proteins with shorter transmembrane domains are modeled to partition into thinner bilayers, whereas proteins with longer transmembrane domains are modeled to partition into thicker bilayers (Bretscher and Munro, 1993; Lundbaek et al., 2003). Because protein distribution is dependent on local lipid composition in this mechanism, concentration of resident proteins in specific Golgi regions (e.g., medial or *trans*) requires only a means for establishing *cis*-to-*trans* lipid gradients. Because these gradients are already a feature of the organization of lipid trafficking in the model, resident protein distributions can be readily explained without invoking additional sorting machinery. This feature of the rapid-partitioning model is demonstrated by simulation of resident protein, SL, and GPL trafficking modules in parallel. Golgi proteins having different preferred SL/GPL environments are found to concentrate in different Golgi cisternae (e.g., *cis*, medial or *trans*) even with continuous movement up and down the stack (Figure 7C; details in Model S10).

We next tested the spatially resolved, rapid-partitioning model with VSVG export data observed in our bulk release (iFRAP) and pulse release (short refill) experiments. When we compared this with data from the iFRAP experiment, we found that the spatially resolved rapid-partitioning model can account for the exponential cargo release kinetic data (Figure 7D; for details, see Model S9).

The Rapid-Partitioning Model Predicts a Cargo Wave upon Temperature Blockade and Release

A potential challenge to the rapid-partitioning model is explanation of the cargo wave seen traversing the Golgi stack in response to a short, low-temperature block and release of membrane traffic (Trucco et al., 2004). Upon release from a short temperature block, VSVG is found to shift its distribution from cisterna to cisterna in a wave-like pattern across the stack as quantified by immunogold labeling and electron microscopy. Previously, this was interpreted as evidence for cisternal progression, with the time for the wave to traverse the Golgi (i.e., 12–16 min) corresponding to the rate of cisternal maturation. In the framework of the rapid-partitioning model, however, the protocol for generating the cargo wave (i.e., 40°C to 15°C for 15 min and then back to 40°C) alters the Golgi's lipid gradient and affects both the distribution of cargo across the cisternae and cargo export rates out of cisternae (Figure 7E). Recent electron microscopy data showing enzymes are disorganized within the Golgi stack at 15°C (Martinez-Alonso et al., 2005) supports this interpretation. To directly address the effect of the temperature block and release protocol effect on cargo and lipid distributions, we applied it to simulations of the rapid-partitioning model.

The simulated behavior of SLs and GPLs during this protocol is shown in Figure 7F (for details, see Model S12). Within 15 min of shifting from 40°C to 15°C, the SL/GPL ratios in all Golgi exit domains begin to approach the ratio characterizing the entire Golgi when steady-state gradients are abolished and the lipids equilibrate in a closed system. Upon shift to 40°C, the SL/GPL ratios in all Golgi export domains begin re-establishing their steady-state levels seen prior to the 15°C incubation period. During this temperature shift, only VSVG molecules that had accumulated in pre-Golgi structures during the 15°C incubation enter the *cis* Golgi. Because this pulse of cargo carries a corresponding wave of GPL, it transiently dilutes the SL in the Golgi, reducing the SL/GPL ratio in each exit domain. Over the succeeding 14 min, therefore, the SL/GPL ratios in each cisternal exit domain drop below steady-state 40°C levels and then gradually return to their steady-state levels.

The simulated behavior of VSVG upon shift to 40°C in the protocol is plotted in Figure 7G. The molecules quickly distribute throughout all cisternae but are initially most concentrated in the first cisterna because it first displays the optimal SL/GPL ratio for VSVG. Over the succeeding 14 min, each cisterna, in turn, becomes the place where VSVG is optimally localized (due to VSVG distributing according to its optimal SL/GPL ratio). A wave of cargo thus appears to traverse the Golgi stack as VSVG molecules move randomly and discover their minimum free energy environment. This wave of cargo repositioning as predicted by the rapid partitioning model is illustrated in Figure 7H, which plots the relative number of molecules in each cisterna at 3, 6, 10, and 17 min after release of a pulse of VSVG from pre-Golgi structures. Thus, the wave of cargo traversing the Golgi stack seen in previous electron microscopy studies (Trucco et al., 2004) can be explained in the rapid-partitioning model without invoking *cis*-to-*trans* movement of cisternae in a cisternal maturation pathway.

The rapid-partitioning model furthermore accounts for other Golgi characteristics. With the model parameters that produce the timing of the cargo wave, cargo preferentially enriches in the *cis*-most cisterna during the first 3 min of cargo entry into the Golgi after the usual 40°C to 32°C temperature shift (Figure S6), which is also observed in a previous immunogold electron microscopy (Bergmann and Singer, 1983). Quantitatively, cargo takes approximately 4–5 min to distribute widely across the Golgi stack, consistent with our electron microscopy results shown in Figure 2B, Figure S2C, and previous observations (Bergmann and Singer, 1983; Griffiths, 2000). Nevertheless, there is no lag in cargo export (see Figure 7D) because cargo molecules can exit from export domains in all cisternae. The rapid-partitioning model accounts for all these results and the cargo wave while simultaneously accounting for other key features of the Golgi (i.e.,

protein and lipid gradients and monoexponential cargo export kinetics). We conclude, therefore, that it is an effective unifying hypothesis for Golgi apparatus organization and function.

DISCUSSION

In this study, we tested several widely accepted versions of cisternal maturation against previous data on polarized Golgi lipid gradients, nonuniform distribution of resident proteins, and the production of cargo waves after a temperature block. These were tested against new data on kinetics of cargo release from the Golgi (unconfounded by continuous entry from the ER) and on partitioning of cargo within the Golgi. Our studies indicate that neither cisternal maturation as classically defined nor any of its modern variations can simultaneously account for all of these data. In their place, we proposed and rigorously tested a new model of intra-Golgi trafficking based on partitioning of transmembrane cargo and enzymes within a two-phase membrane system. In this model, the stack-like organization of the Golgi, combined with the requirement of vesicular or tubule cargo transport across it (which prevents the system from becoming well mixed) and with the partitioning of lipids between two domains allows molecules in the system to sort spatially.

Simulation and experimentally testing of the rapid-partitioning model generates monoexponential export kinetics of VSVG-YFP and other major features of the Golgi. We find a gradient in SL/GPL composition, with the ratio lowest in the *cis* cisterna and highest in the *trans* cisterna. Resident proteins with different SL/GPL preferences enrich in different cisternae within the Golgi despite processing enzymes and cargo continuously circulating up and down the stack. Finally, the simulations reveal a cargo wave pattern across the Golgi stack in response to a short, low-temperature block and release of membrane traffic, consistent with that observed in electron microscopy experiments (Trucco et al., 2004). The model and parameter values thus comprise a useful working hypothesis that can be challenged to account for future results as new information about Golgi structure and function emerges.

At the same time, the model can be seen as an organizing principle for the molecular machinery that previous studies have associated with the Golgi pathway. For example, phosphatidylinositol 4-phosphate and diacylglycerol are known to be required for Golgi to plasma membrane transport (Bard and Malhotra, 2006). Their respective effectors, phosphatidylinositol-4-phophate adaptor proteins (FAPPs) and protein kinase D, modulate levels of specific lipids in the Golgi and lead to recruitment and/or activation of fission-inducing proteins (Bard and Malhotra, 2006; D'Angelo et al., 2007). Within the partitioning model, this could be a consequence of specific SL/GPL concentrations facilitating the spatial organization of these molecules. Similarly, Arf1, coatomer, Arf1-GAP, and their effectors, which regulate retrograde transport to the ER, would be dependent on the existence of specific SL/GPL concentrations for facilitating their temporal-spatial assembly. In contrast, clathrin and GGA proteins, which sort molecules into vesicles destined for lysosomes, would be predicted to act at sites distinct from SL/GPL-rich export domains budding off vesicles toward the plasma membrane. Consistent with this, high-resolution, tomographic imaging of the Golgi has shown that the TGN produces exclusively clathrin-coated buds, whereas other cisterna display only non-clathrin-coated buds (Ladinsky et al., 1999). Because clathrin is involved exclusively in packaging products destined for the endosome/lysosome pathway, association with the *trans*-most cisternae suggests that this cisternae packages molecules for the lysosomal pathway rather than the plasma membrane and thus acts separately than the rest of the Golgi. Supporting this interpretation is our observation that TGN38 did not colocalize with VSVG during BFA treatment.

The model can also account for intra-Golgi transport of small and large soluble cargos. Small, soluble cargos circulate through the luminal volume of the Golgi system, freely moving into carriers that bud out toward the plasma membrane. Large insoluble cargos (i.e., Procollagen), on the other hand, are too large to pass freely in this manner and so use a different mechanism. A possible explanation is that once such cargos become too large to move into the vesicles and tubules mediating transport between cisternae, they gain affinity for export domain lipids. Partitioning of these lipids around the aggregates would then lead to the formation of a transport carrier. Cisternal movement (e.g., progression) could additionally play a role in distributing the Procollagen aggregates across the stack, but not for the purpose of export. Instead, the export of Procollagen aggregates would be dependent on the kinetics of exit domain lipid partitioning around these aggregates, a process compatible with the experimentally observed monoexponential export kinetics of Procollagen.

In summary, our methods and tools for formulation and testing intra-Golgi transport models suggest that the mammalian Golgi apparatus comprises a two-dimensional gradient in lipid composition generated by two physical processes at work simultaneously. One process is the physical distribution of proteins and lipids as a consequence of their entry and exit fluxes, which establishes their steady-state distribution in the cisternal membranes of the Golgi. The second process is the partitioning into domains on the basis of physical properties of the individual membrane components. With these two processes operating across a two-dimensional structure of interconnected cisternae that may be progressing, we demonstrate by simulation and experimental evidence that a membrane system can arise with all the key characteristics of the Golgi apparatus.

EXPERIMENTAL PROCEDURES

Plasmid Constructs

Strategies for construction of fluorescent protein chimeras are outlined in the Supplemental Data.

Cell Culture

COS 7 cells, NRK cells, human fibroblast cells, and chick embryonic fibroblast cells were grown in Lab-Tek chambers with #1.0 borosilicate cover glasses (Nalge Nunc International, Naperville, IL) or on #1.5 round cover glasses (A. Daigger & Company, Wheeling, IL). Transfections were performed with FuGENE 6 transfection reagent (Roche, Indianapolis, IN). Imaging medium was DMEM containing 25 mM HEPES (pH 7.5) (Biosource International, Rockville, MD), or CO2 independent medium (Invitrogen, Carlsbad, CA).

Fluorescence Microscopy

Imaging of CFP, GFP, and YFP was performed in multitracking mode on a Zeiss LSM510, a Zeiss LSM510 META, or a Zeiss LSM510 ConfoCor 2 laser scanning confocal microscope (Carl Zeiss, Thornwood, NY) with a 25× Plan

NeoFluar 0.8 NA objective, a 40× Plan NeoFluar 1.3 NA objective, or a 63× Plan Apochromat 1.4 NA objective. Imaging was also performed with an Olympus FV1000 Fluoview laser scanning confocal microscope with a 60× Plan Apochromat 1.4 NA objective.

Image Analysis

Images were collected in 8 bit or 12 bit mode and analyzed with Zeiss LSM510 software (Carl Zeiss, Thornwood, NY) or converted into 8 bit and analyzed with NIH Image 1.62 or ImageJ 1.34 (National Institutes of Health, Bethesda, MD). Mean pixel values of the background (a region selected outside of the cell) were subtracted from the mean pixel value of the region of interests inside the cell or a region of interest encompassing the entire cell. The mean pixel value of a region of the plasma membrane was subtracted from the mean VSVG pixel value in the Golgi region to remove the plasma membrane contribution from the quantification. Imaging conditions were chosen to minimize photobleaching during the experiments, and the loss in fluorescence was normalized by the entire cell fluorescence, which was quantified from the ~22 μm optical sections obtained with the 25× 0.8 NA objective.

Electron Microscopy

VSVG-GFP-expressing cells were fixed for immuno-EM at the end of the 40°C block or at different times after its release as described (Polishchuk et al., 2000). Then cells were incubated with polyclonal anti-GFP antibody (Abcam, UK) overnight and subsequently with anti-rabbit Fab' fragment nanogold conjugates (NanoProbes) enhanced then with GoldEnhance kit (NanoProbes). Epon embedding and sectioning of the gold-labeled cells was performed as reported earlier (Polishchuk et al., 2000). Sections were then analyzed under Philips Tecnai-12 electron microscope (Philips, Einhoven, The Netherlands) equipped with Analysis software.

Kinetic Analysis and Modeling

All models and model variants were formulated and managed with the ProcessDB software (Integrative Bioinformatics, www.integrativebioinformatics.com) and exported to Berkeley Madonna (www.berkeleymadonna.com) for solution and parameter optimization. Detailed technical information on the models and computational techniques used in this work is provided in the Supplemental Data. We provide the text of model definitions, native files for Berkeley Madonna as exported from ProcessDB, and explanatory comments that should permit interested groups to reproduce and evaluate these results.

SUPPLEMENTAL DATA

Supplemental Data include Model Descriptions, Supplemental Results and Discussion, Supplemental Experimental Procedures, Supplemental References, ten figures, one table, and six movies and can be found with this article online at http://www.cell.com/cgi/content/full/133/6/1055/DC1/.

ACKNOWLEDGMENTS

We thank Nihal Altan-Bonnet, Rachid Sougrat, Suliana Manley, Markus Elsner, and Wei Lui for assistance in preparing this manuscript. We thank Alberto Luini and Alexander Mironov (Consorzio Mario Negri Sud, Italy) for sharing the Procollagen-GFP cDNA, for sharing unpublished observations, and for helpful discussions. We thank David Piston, Atsushi Miyawaki, Julie Donaldson, Frederick Suchy, and Colin Hopkins for sharing reagents. This work was funded in part by U.S.-Israel Binational Science Foundation (BSF) grant #2005281 to K.H. and J.L.S. The kinetic modeling and data analysis reported here were supported in part by NIH R01GM079305 to R.D.P. and Integrative Bioinformatics (IBI). R.D.P. is cofounder of IBI. The ProcessDB software used in this study was developed by IBI with support from NIH SBIR grants R43GM066611 and R44GM066611.

Received: May 18, 2007
Revised: November 15, 2007
Accepted: April 24, 2008
Published: June 12, 2008

REFERENCES

Bard, F., and Malhotra, V. (2006). The formation of TGN-to-plasma-membrane transport carriers. Annu. Rev. Cell Dev. Biol. *22*, 439–455.

Bergmann, J.E., and Singer, S.J. (1983). Immunoelectron microscopic studies of the intracellular transport of the membrane glycoprotein (G) of vesicular stomatitis virus in infected Chinese hamster ovary cells. J. Cell Biol. *97*, 1777–1787.

Bonfanti, L., Mironov, A.A., Jr., Martínez-Menárguez, J.A., Martella, O., Fusella, A., Baldassarre, M., Buccione, R., Geuze, H.J., Mironov, A.A., and Luini, A. (1998). Procollagen traverses the Golgi stack without leaving the lumen of cisternae: Evidence for cisternal maturation. Cell *95*, 993–1003.

Bretscher, M.S., and Munro, S. (1993). Cholesterol and the Golgi apparatus. Science *261*, 1280–1281.

D'Angelo, G., Polishchuk, E., Di Tullio, G., Santoro, M., Di Campli, A., Godi, A., West, G., Bielawski, J., Chuang, C.C., van der Spoel, A.C., et al. (2007). Glycosphingolipid synthesis requires FAPP2 transfer of glucosylceramide. Nature *449*, 62–67.

Dunphy, W.G., and Rothman, J.E. (1983). Compartmentation of asparagine-linked oligosaccharide processing in the Golgi apparatus. J. Cell Biol. *97*, 270–275.

Fries, E., Gustafsson, L., and Peterson, P.A. (1984). Four secretory proteins synthesized by hepatocytes are transported from endoplasmic reticulum to Golgi complex at different rates. EMBO J. *3*, 147–152.

Gkantiragas, I., Brugger, B., Stuven, E., Kaloyanova, D., Li, X.Y., Lohr, K., Lottspeich, F., Wieland, F.T., and Helms, J.B. (2001). Sphingomyelin-enriched microdomains at the Golgi complex. Mol. Biol. Cell *12*, 1819–1833.

Glick, B.S., Elston, T., and Oster, G. (1997). A cisternal maturation mechanism can explain the asymmetry of the Golgi stack. FEBS Lett. *414*, 177–181.

Griffiths, G. (2000). Gut thoughts on the Golgi complex. Traffic *1*, 738–745.

Holthuis, J.C., Pomorski, T., Raggers, R.J., Sprong, H., and Van Meer, G. (2001). The organizing potential of sphingolipids in intracellular membrane transport. Physiol. Rev. *81*, 1689–1723.

Kepes, F., Rambourg, A., and Satiat-Jeunemaitre, B. (2005). Morphodynamics of the secretory pathway. Int. Rev. Cytol. *242*, 55–120.

Killian, J.A. (1998). Hydrophobic mismatch between proteins and lipids in membranes. Biochim. Biophys. Acta *1376*, 401–415.

Ladinsky, M.S., Mastronarde, D.N., McIntosh, J.R., Howell, K.E., and Staehelin, L.A. (1999). Golgi structure in three dimensions: Functional insights from the normal rat kidney cell. J. Cell Biol. *144*, 1135–1149.

Lippincott-Schwartz, J., Yuan, L., Tipper, C., Amherdt, M., Orci, L., and Klausner, R.D. (1991). Brefeldin A's effects on endosomes, lysosomes, and TGN suggest a general mechanism for regulating organelle structure and membrane traffic. Cell *67*, 601–616.

Losev, E., Reinke, C.A., Jellen, J., Strongin, D.E., Bevis, B.J., and Glick, B.S. (2006). Golgi maturation visualized in living yeast. Nature *441*, 1002–1006.

Lundbaek, J.A., Andersen, O.S., Werge, T., and Nielsen, C. (2003). Cholesterol-induced protein sorting: an analysis of energetic feasibility. Biophys. J. *84*, 2080–2089.

Marsh, B.J., Volkmann, N., McIntosh, J.R., and Howell, K.E. (2004). Direct continuities between cisternae at different levels of the Golgi complex in glucose-stimulated mouse islet beta cells. Proc. Natl. Acad. Sci. USA *101*, 5565–5570.

Martinez-Alonso, E., Egea, G., Ballesta, J., and Martinez-Menarguez, J.A. (2005). Structure and dynamics of the Golgi complex at 15 degrees C: Low temperature induces the formation of Golgi-derived tubules. Traffic *6*, 32–44.

Matsuura-Tokita, K., Takeuchi, M., Ichihara, A., Mikuriya, K., and Nakano, A. (2006). Live imaging of yeast Golgi cisternal maturation. Nature *441*, 1007–1010.

Melkonian, M., Becker, B., and Becker, D. (1991). Scale formation in algae. J. Electron Microsc. Tech. *17*, 165–178.

Mogelsvang, S., Marsh, B.J., Ladinsky, M.S., and Howell, K.E. (2004). Predicting function from structure: 3D structure studies of the mammalian Golgi complex. Traffic *5*, 338–345.

Nagai, T., Ibata, K., Park, E.S., Kubota, M., Mikoshiba, K., and Miyawaki, A. (2002). A variant of yellow fluorescent protein with fast and efficient maturation for cell-biological applications. Nat. Biotechnol. *20*, 87–90.

Nehls, S., Snapp, E.L., Cole, N.B., Zaal, K.J.M., Kenworthy, A.K., Roberts, T.H., Ellenberg, J., Presley, J.F., Siggia, E., and Lippincott-Schwartz, J. (2000). Dynamics and retention of misfolded proteins in native ER membranes. Nat. Cell Biol. *2*, 288–295.

Orci, L., Montesano, R., Meda, P., Malaisse-Lagae, F., Brown, D., Perrelet, A., and Vassalli, P. (1981). Heterogeneous distribution of filipin–cholesterol complexes across the cisternae of the Golgi apparatus. Proc. Natl. Acad. Sci. USA *78*, 293–297.

Orci, L., Ravazzola, M., Volchuk, A., Engel, T., Gmachl, M., Amherdt, M., Perrelet, A., Söllner, T.H., and Rothman, J.E. (2000). Anterograde flow of cargo across the Golgi stack potentially mediated via bidirectional "percolating" COPI vesicles. Proc. Natl. Acad. Sci. USA *97*, 10400–10405.

Polishchuk, R.S., Polishchuk, E.V., Marra, P., Alberti, S., Buccione, R., Luini, A., and Mironov, A.A. (2000). Correlative light-electron microscopy reveals the tubular-saccular ultrastructure of carriers operating between Golgi apparatus and plasma membrane. J. Cell Biol. *148*, 45–58.

Presley, J.F., Cole, N.B., Schroer, T.A., Hirschberg, K., Zaal, K.J.M., and Lippincott-Schwartz, J. (1997). ER-to-Golgi transport visualized in living cells. Nature *389*, 81–85.

Rabouille, C., Hui, N., Hunte, F., Kieckbusch, R., Berger, E.G., Warren, G., and Nilsson, T. (1995). Mapping the distribution of Golgi enzymes involved in the construction of complex oligosaccharides. J. Cell Sci. *108*, 1617–1627.

Rizzo, M.A., Springer, G.H., Granada, B., and Piston, D.W. (2004). An improved cyan fluorescent protein variant useful for FRET. Nat. Biotechnol. *22*, 445–449.

Roth, J., Taatjes, D.J., Weinstein, J., Paulson, J.C., Greenwell, P., and Watkins, W.M. (1986). Differential subcompartmentation of terminal glycosylation in the Golgi apparatus of intestinal absorptive and goblet cells. J. Biol. Chem. *261*, 14307–14312.

Slot, J.W., and Geuze, H.J. (1983). Immunoelectron microscopic exploration of the Golgi complex. J. Histochem. Cytochem. *31*, 1049–1056.

Sun, A.Q., Swaby, I., Xu, S., and Suchy, F.J. (2001). Cell-specific basolateral membrane sorting of the human liver Na(+)-dependent bile acid cotransporter. Am. J. Physiol. Gastrointest. Liver Physiol. *280*, G1305–G1313.

Trucco, A., Polishchuk, R.S., Martella, O., Di Pentima, A., Fusella, A., Di Giandomenico, D., San Pietro, E., Beznoussenko, G.V., Polishchuk, E.V., Baldassarre, M., et al. (2004). Secretory traffic triggers the formation of tubular continuities across Golgi sub-compartments. Nat. Cell Biol. *6*, 1071–1081.

van Meer, G., and Sprong, H. (2004). Membrane lipids and vesicular traffic. Curr. Opin. Cell Biol. *16*, 373–378.

Volchuk, A., Amherdt, M., Ravazzola, M., Brügger, B., Rivera, V.M., Clackson, T., Perrelet, A., Söllner, T., Rothman, J.E., and Orci, L. (2000). Megavesicles implicated in the rapid transport of intracisternal aggregates across the Golgi stack. Cell *102*, 335–348.

White, J., Keller, P., and Stelzer, E.H. (2001). Spatial partitioning of secretory cargo from Golgi resident proteins in live cells. BMC Cell Biol. *2*, 19.